Digest Journal of Nanomaterials and Biostructures Vol. 11, No. 3, July - September 2016, p. 833 - 843

STUDY OF PHYSICAL PROPERTIES OF BSA:PEDOT-PSS THIN FILM OBTAINED BY SPIN-COATING

O. BRÎNCOVEANU [a,b], A. IOANID [a], S. IFTIMIE [a], J. AL-ZANGANAWEE [b]
M. ENACHESCU [b,c], S. ANTOHE [a,c,*]
[a]*Faculty of Physics, University of Bucharest, 077125, Romania*
[b]*Center for Surface Science and Nanotechnology, University Politehnica of Bucharest, 060042 Romania*
[c]*Academy of Romanian Scientists, Bucharest, 050094, Romania*

Bovine serum albumin:Poly(3,4-ethylenedioxythiophene) – poly(styrenesulfonate**)** (BSA:PEDOT-PSS[1:1]) solution was prepared and deposited as bioactive layer onto silicon (100) substrates, covered with a thin silver layer deposited by pulsed laser deposition (PLD). Atomic force microscopy (AFM) analysis such as topography image, electrostatic images and force – distance facilities, as well as Resonance Raman (RR) spectroscopy have been used to identify the morphological and compositional features of the bioactive layer, but also to evaluate the surface activity. Our results coming, from a comparative study of each component, BSA and PEDOT-PSS, and of BSA:PEDOT-PSS[1:1] mixture, showed both inherited and new physical properties of bioactive layer.

(Received June 2, 2016; Accepted August 8, 2016)

Keywords: Bioactive layer, Hydrophobic surface properties, Adhesion force, Biosensors, Resonance Raman

1. Introduction

AFM is a useful tool for direct measurements of microstructural surface parameters and intermolecular forces of thin films. By this technique, nN range forces can be measured under physiological conditions, facilitating the study of many biological processes like drug/protein, protein/protein, protein/polymer interactions and other associated phenomena [1], basic of biodetection applications like biomaterials development [2], biosensor and drug design [3].

Scanning force microscopy (SFM) provides a simultaneous image of surface morphology and various physical forces and make possible to correlate the topography with physical properties. Electrostatic force microscopy (EFM), which is an extension of AFM imaging is used to perform nondestructive electrostatic force measurements between conductive AFM tip and surface, providing the electrical (charge or potential) surface properties. These forces govern chemical and physical processes on which many nanotechnology applications are based [4]. The tip – surface electrostatic interactions, given by long range Coulomb forces [5], depends on tip shape and cantilever geometry. Thus, $F \sim -dC/2dz \cdot V^2$, where C is tip – sample capacitance, z is tip – sample distance and V is tip – sample electric potential gradient. EFM images were recorded as tip- sample surface potential gradient distributions, at room temperature, in controlled environment conditions, to compare the mixture surface properties with individual protein and polymer ones.

Operating in contact mode, the tip – surface interaction are mainly due to van der Waals forces, and depends on the state of polarization, polarizability and elastic properties of the explored surface. In this case, the force – distance (F(z)) curve was recorded in "snap-off" range, at room temperature, in controlled environment conditions, to evaluate the van der Waals interaction for the mixture and individual protein and polymer surface.

It is known that the Raman scattering is a non-invasive method suitable for molecular multi-component structures, which identifies the type and abundance of the interatomic bonds. The

* Corresponding author: santohe@solid.fizica.unibuc.ro

resonance Raman (RR) spectrum gives the inelastic scattered radiation from atoms of explored surface under laser excitation λ_{laser}, $h\nu_{scattered} = h\nu_{laser} \pm h\nu_{vibrational}$. The recording occurs in atom de-excitation after $h\nu_{laser}$ photon absorption, during which part of energy is consumed in vibrational excitations associated to inter-atomic bonds. The difference between the excitation and scattered photon energy gives the Raman shift. The peak position characterizes the vibrational energy associated with a bond or a group of atom bonds, while the peak intensity reflects the bond type abundance. Usually, for compounds, a narrow peak is associated with one vibration mode only, while a broad one reflects an overlapping situation of several vibrations and has to be decompose to identify the peaks corresponding to overlapping modes.

In our paper we present experimental results consisting in AFM measurements (topography and potential images, profile curves, force – distance curves) and RR spectra obtained for BSA, PEDOT-PSS and BSA:PEDOT-PSS[1:1] mixture films. BSA has been selected as protein component because is homologue to human albumin (HSA). It is known that the serum albumin is one of the main proteins of biological fluid, with important physiological functions, which makes it suitable for biomedical applications [6,7]. BSA has good stability in aqueous solutions, facilitating various interactions [8,9,10]. PEDOT-PSS has been selected as polymer component taking into account some suitable properties, like low band-gap, high conductivity, high absorption coefficient, mechanical flexibility as thin film, high environmental stability and low cost fabrication. BSA was incorporated in PEDOT-PSS matrix as counter-ions, by mixing. The BSA:PEDOT-PSS[1:1] mixture showed new physical properties combining the bioactivity of BSA and the mechanical stability of PEDOT-PSS [11].

The analysis of our results enables BSA:PEDOT-PSS[1:1] mixture structural modeling as a new molecule consisting from BSA molecule as core embedded of PEDOT chains, via predominantly dipole – dipole interactions. The surface of our fabricated molecule has good adhesion efficiency, in order to recognize and immobilize some target biomolecules, as main function of biomedical devices.

2. Experimental

2.1 Materials

BSA:PEDOT-PSS[1:1] was synthesized by mixing BSA and PEDOT-PSS equimolar solutions, both materials purchased from Sigma-Aldrich. Thus, the BSA solution was prepared using lyophilized powder with deionized water with ~66kDa, pH 7.0, 0.02 M, ≥95% (agarose gel electrophoresis) and the PEDOT-PSS solution has the concentration 1.3 wt.% (PEDOT content 0.5 wt.%; PSS content 0,8 wt. %), 0.02 M, 1 S/cm. Afterwards, the BSA, PEDOT-PSS and BSA:PEDOT-PSS[1:1] films were obtained by spin coating on a thin compact silver layer supported by silicon (100) wafer obtained by pulsed laser deposition. The BSA:PEDOT-PSS[1:1]/Ag/Si film structure properties are compared to those of individual Ag/Si, BSA/Ag/Si, PEDOT-PSS/Ag/Si film structures.

2.2 Apparatus

AFM and EFM measurements were perform at ambient atmosphere (t=23ºC, RH~32%) for the same Ag/Si, BSA/Ag/Si, PEDOT-PSS/Ag/Si, BSA:PEDOT-PSS[1:1]/Ag/Si films both in non-contact mode using a silicon/Pt-coated cantilever with the spring constant of 17 N/m and resonance frequency of 230 kHz for topography and electrostatic images capture and in contact mode using a silicon tip with spring constant of 0.26 N/m and resonance frequency of 19 kHz for recording of F(z) curves. All the measurements were performed on Solver Next (NT-MDT) AFM equipment. For quantitative determinations of molecular mixture organization, we used Raman scattering technique. The resonant Raman (RR) spectrum was recorded for each BSA/Ag/Si, PEDOT-PSS/Ag/Si, BSA:PEDOT-PSS[1:1]/Ag/Si films surface by Micro-Raman confocal Spectroscopy technique (LabRam HR – Horiba equipment) at room temperature, using a green (532 nm) laser beam.

3. Results and discussions

3.1. AFM and EFM analysis of BSA:PEDOT-PSS thin film

AFM and EFM comparative analysis were performed on Ag/Si, BSA/Ag/Si, PEDOT-PSS/Ag/Si, BSA:PEDOT-PSS[1:1]/Ag/Si films surface. The Ag film is used as backside of the active layer. As it is known, the EFM technique characterizes the electrical properties of exposed materials surface. A conductive tip interacts with the sample surface through Colombian forces, these interactions change the tip oscillation amplitude related to the gradient of the electric field between the tip and the sample surface [1,12], so the cantilever resonance frequency shift Δf due to the tip-sample surface electrostatic forces can be expressed as $\Delta f \propto \frac{\partial F}{\partial z} = -\frac{\partial^2 U}{\partial z^2} = \frac{\partial^2 C}{\partial z^2}(V_{tip} - V_{surface})^2$, were U is the tip – sample surface voltage, C is the tip – surface sample capacitance, z is the height above the sample surface, V_{tip} is the potential applied to the tip, $V_{surface}$ is the surface local potential. The topography images were acquired in non-contact mode to avoid unexpected charge injections from the tip to the surface. The EFM is a double-pass technique, during the first-pass the surface topography is determinate in non-contact mode; then, in the second-pass, the tip is lifted above the sample surface at the height Δz = 80 nm and an DC bias voltage V_{tip} of 1V is applied between the tip and sample surface, while the piezo-tube ensures the tip oscillation at its resonance frequency. Information provided by the simultaneously topographic and electrical images allows quantitative studies for each sample and comparative assessment of the above nanosided active layers' surface.

In Figure 1 are represented the topography (left), lateral distance (middle) and electrostatic images (right) for all samples. The topography images show that all the three layers have uniform distribution and the profile height is around 1.6 nm, 4.0 nm and 2.0 nm, for BSA (a), PEDOT-PSS (b) and BSA:PEDOT-PSS[1:1] (c) layers surface, respectively. Table 1 contains the values of the usual morphological parameters: the root mean-square roughness (RMS), arithmetic average roughness (RA), Skewness parameter (S_{Sk}), peak-to-valley (Z), obtained as average values from a minimum of three independent images data, for different regions on each sample, using Gwyddion modular software: $RMS = R_q = \left(\sum_{i=1}^{N}\left[\frac{(h_i-\bar{h})^2}{N}\right]\right)^{1/2}$, $RA = \sum_{i=0}^{N}\frac{h_i}{N}$, $R_{Skew} = \frac{1}{NR_q^3}\sum_{i=1}^{N}\left(h_i - \bar{h}\right)^3$.

Table 1. Values of morphological parameters of Ag/Si, BSA/Ag/Si, PEDOT-PSS/Ag/Si and BSA:PEDOT-PSS/Ag/Si films

Sample	RMS (nm)	RA (nm)	Z (nm)	SSkew	Dsurface (nm)	Axial ratio
Ag/Si	1.87	1.47	10.4	0.72	-	-
BSA/Ag/Si	0.23	0.19	1.82	0.01	55	0.033
PEDOT-PSS/Ag/Si	0.75	0.60	4.55	0.17	71	0.064
BSA:PEDOT-PSS/Ag/Si	0.24	0.19	2.17	0.04	57	0.038

Taking into account the morphological parameter definitions, the analysis of the above values leads to the following remarks: i) the silver film (a) has high roughness (1.87 nm) coming from high peaks with high asymmetry (0.72). These values characterize an exposed surface film favorable for adhesion of solvent molecules; ii) the BSA deposited film on the silver film (b) has lower roughness (0.23nm) and is almost symmetric (0.01), while the PEDOT-PSS deposited film on the metallic film (c) is asymmetric (0.17) and has a roughness of three times higher than BSA (0.75 nm). These results proved that BSA molecules in solution can adhere easily to the exposed metal film, leveling the metallic surface and generating a uniform, almost symmetrical film with low roughness, which may be associated with the elongated rather than the globular shape of the deposited BSA molecules [13, 14].

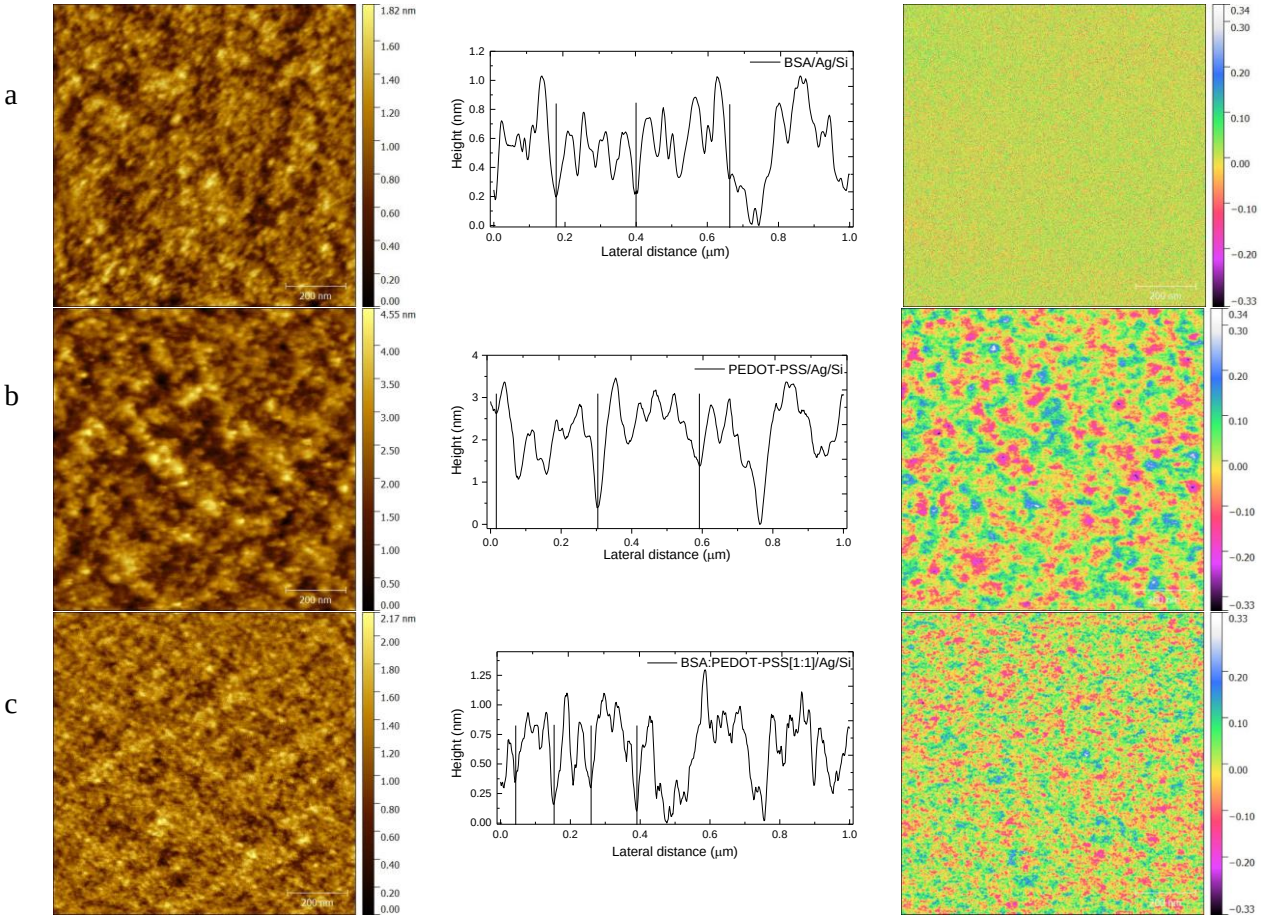

Fig. 1. AFM topography (left), lateral distance (middle) and electrostatic images (right) of a) BSA/Ag/Si, b) PEDOT-PSS/Ag/Si, c) BSA:PEDOT-PSS[1:1]/Ag/Si

The topography image of the BSA:PEDOT-PSS[1:1] film surface (Figure 1c) shows a homogeneous film with values of roughness (0.24) and asymmetry (0.04) higher than those of the BSA film, but much lower than those of PEDOT-PSS film. These considerations lead to the assumption that the film surface contains new molecular formations with linear dimensions greater than the BSA molecules but smaller than PEDOT-PSS particle.

It is known that by changing the configuration, the elongated BSA molecules expose a high number of hydrophobic groups and free valences of sulfur atoms from broken disulfide bonds. Thus, the stability of the protein layer is provided by the increase of hydrophobic interactions with the metallic film and by the chain of S-Ag links generated on the film surface [15], which ensure a stable and compact protein layer deposition. With the same considerations, the PEDOT-PSS film has a higher and asymmetric roughness, characterizing a film generated by large PEDOT-PSS particles deposition [16].

The electrostatic images show the values (normalized to the potential applied to the tip value) of the potential generated by the local charge distribution on the explored surface. The areas marked with blue and red correspond to positive and negative charge, respectively and yellow represent neutral areas (Figure 1, right). As can be observed, while the BSA (a) layer surface is almost neutral (the areas marked with red and blue are very small and the yellow areas are prevalent), both the PEDOT-PSS (b) and BSA:PEDOT-PSS[1:1] (c) layer surfaces have large negative (red) and positive (blue) charged areas. Both the negative and positive charged areas are broader for PEDOT-PSS layer surface than the BSA:PEDOT-PSS[1:1] layer surface, whose neutral areas are broader. Moreover, while for PEDOT-PSS layer surface the negative charged areas are broader than the positive charged, for BSA:PEDOT-PSS[1:1] layer surface this

distribution is reversed, indicating that the surface of the mixture is more reducing than that of polymer only.

3.2. Force – distance measurements

F(z) measurements were performed on Ag/Si, BSA/Ag/Si, PEDOT-PSS/Ag/Si, BSA:PEDOT-PSS[1:1]/Ag/Si film surfaces. Operating in contact mode, these forces are of van der Waals type, and for the same tip, depend on the state of polarization, polarizability and elastic properties of the explored molecule surface. Thus, the F(z) analysis provide the information about the local surface explored molecules [17] properties such as elasticity, adhesion, charge density. The force F (nN) between tip and surface can be calculated as $F = k \times \Delta L$, where k is the cantilever spring constant (0.26 N/m) and ΔL is the deflection distance (nm) [17, 18, 19].

In order to evaluate the elastic constant of the surface has been used the F(z) value as the average value from twenty force curves acquired for each sample, for different surface places in the snaps-off region [20]. It was observed that for all samples both the topography and F(z) are stable and reproducible for repeated AFM operation.

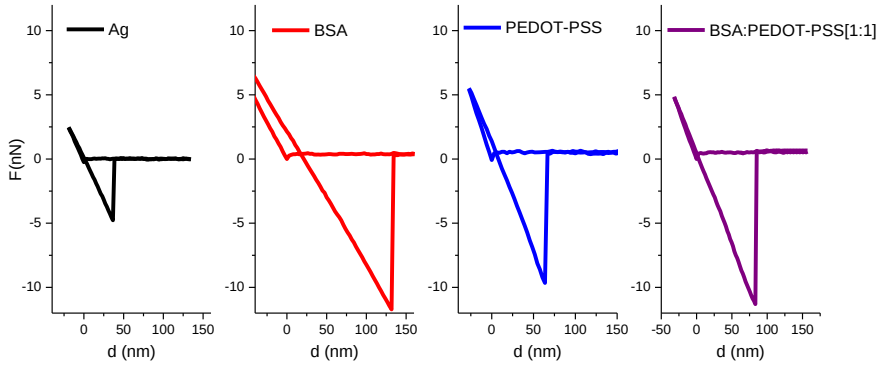

Fig. 2. F(z) analysis for Ag/Si (black), BSA/Ag/Si (red), PEDOT-PSS/Ag/Si (blue) and BSA:PEDOT-PSS/Ag/Si (purple)

In Fig. 2 are represented the F(z) curves for all fabricated thin films and in Table 2 are presented the calculated values of: maximum value of tip/surface attraction force F_{max}, tip/surface distance d_o for F_{max} and effective spring constant k ($k=\Delta F/\Delta d$, $1/k=1/k_{tip}+1/k_{surface}$) of the elastic tip/surface interaction.

Table 2. Calculated values of main parameters characterizing force-distance measurements

Film	F_{max} (nN)	d_o (nm)	k (N/m)	$\sigma_{nanoparticle} = 2d_0 - \sigma_{tip}$ (nm)
Ag/Si	4.80	36.0	-	-
BSA/Ag/Si	11.80	130.5	0.098	$2x130.5-\sigma_{dip}$
PEDOT-PSS/Ag/Si	9.65	63.7	0.136	$2x63.7-\sigma_{dip}$
BSA:PEDOT-PSS[1:1]/Ag/Si	11.30	83.3	0.170	$2x83.3-\sigma_{dip}$

3.3 Raman studies

The RR spectra were recorded for individual BSA, PEDOT-PSS, BSA:PEDOT-PSS[1:1] films, with λ_{excit} = 532 nm in the 350 – 1800 cm^{-1} range with the acquisition time of 10 sec/spectrum/window and 15 spectra acquired. The RR spectra are shown in Fig. 3a.

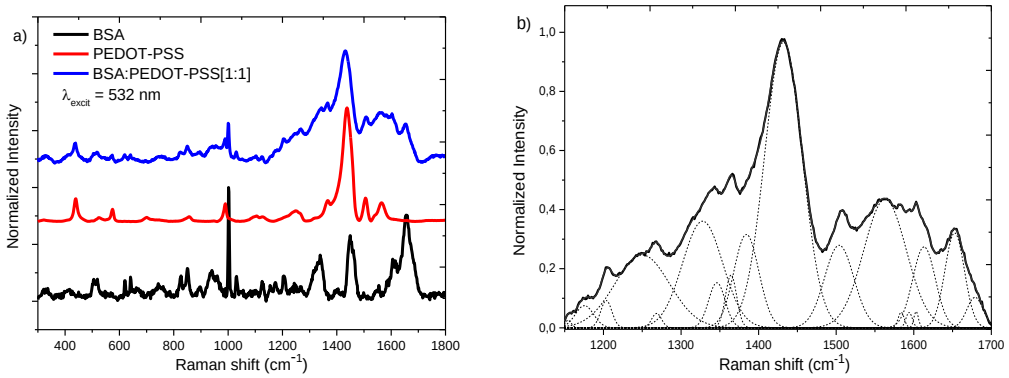

Fig. 3. RR spectra using $\lambda_{excit} = 532$ nm laser: a) As recorded BSA (black line), PEDOT-PSS (red line) BSA:PEDOT-PSS[1:1] (blue line);b) Deconvolution of BSA:PEDOT-PSS[1:1] film surface RR spectrum in the Amide I band range.

Table 3. The main Raman peaks and their assignment for the BSA, PEDOT-PSS and BSA:PEDOT-PSS[1:1] films.

BSA:PEDOT-PSS[1:1]		BSA			PEDOT-PSS		
Recorded (cm^{-1})	Deconvoluted (cm^{-1})	Recorded (cm^{-1})	Assignment [21-23]		Recorded (cm^{-1})		Assignment [24,25]
1655	1655	1656	1656	Amide I	-	-	-
1604	1606	1610	1620	Side chains	-	-	-
1562	1561	1554	1554	Trp	1564	1563	PSS
1509	1508	-	-	-	1510	1532	PEDOT $C_\alpha = C_\beta$ (intra-chain)
1432	1432	1449	1450	Backbone	1438	1425	PEDOT $C_\alpha = C_\beta$ (-O) (intra-chain)
1366	1368	-	-	-	1367	1367	PEDOT C_β - $C_{\beta'}$ (inter-chain)
1340	1320	1340	1340	Trp	-	-	-
1267	1266	-	-	-	1256	1256	PEDOT C_α - $C_{\alpha'}$ (inter-ring)
1205	-	1205	1240	Amide III	-	-	-
-	-	1174	1174	Try	-	-	-
1125	-	1125	1126	Trp	1132	1136	PEDOT C-O-C (intra-ring)
1031	-	1031	1010	Trp	1100	1093	PSS
1000	-	1001	1002	Phe	-	-	-
989	-	-	-	-	989.9	989	PSS
940	-	940	941	Backbone	-	-	-
850, 827	-	850, 827	850, 830	Tyr	-	-	-
-/-	-	760	760	Trp	701	701	PSS
640, 620	-	640, 620	620,640	Phe	-	-	-
576	-	-	-	-	576	577	PEDOT C-S-C (intra-ring)
510	-	510	510	Cys	523.9	522	PEDOT
438	-	-			438	437	PEDOT S-S (inter-ring)

The RR spectrum of PEDOT-PSS film shows peaks with significant intensity associated to the backbone polymer chain rings and inter-chains bond vibrations, in the same range of both the Amide I energy band associated to the backbone protein chain peptide unit and of the energy bands associated to tryptophan (Trp), tyrosine (Tyr), phenylalanine (Phe) aromatic amino acids of BSA. Peaks associated to side-chain SO_2 bending vibrations have energies in the same range of S – S bond vibrations in BSA.

The RR spectrum of BSA:PEDOT-PSS[1:1] film shows a structured broadband in the Amide I energy range, 1200 cm^{-1}-1700 cm^{-1}, and some narrow peaks in both the aromatic amino acids and S-S bonds energy range. Fig. 3(b) highlights the structure of this large band obtained using Gauss function deconvolution [26].

4. Disscusions

All previous experimental results converge to the conclusion that the protein-polymer composite (BSA:PEDOT-PSS[1:1]) has a new molecular organization, distinct from both the protein and polymer. To retrieve the stability conditions and the characteristics of this new molecule, it must be considered the molecular structural and electrical charge characteristics of the two components, which favor this stable structural association.

BSA is a globular protein, of 66300 Da molecular weight, having a low content of polar amino acids (i.e., Trp, Tyr, Phe), but a high content of charged amino acids (both cationic: arginine, lysine, glutamine, aspargines, hystidine, and anionic: glutamic acid, aspartic acid) and 35 cysteines, from which 34 form 17 S-S bounds and one free. Thus, the BSA has 185 ionized groups in solution per molecule, activated in zwitterions condition at the isoelectric point pI = 4.7 – 4.9 in PBS buffer normal solution. For pH < pI the BSA molecule is positively, while for pH > pI is negatively charged, having 15 ionized groups per molecule at pH ~ 7.0 [27,28]. Another characteristic of interest for understanding the protein interaction mechanisms is the associated electric dipole moment of the molecular structure. Thus, the α-helix component contributes with p = 3.5 x (N-1)D/helix, oriented along the helix, and the β-sheet with $p = 3.5x(N'-1)^{1/2}$/sheet chain, perpendicular to the chain, where N and N' are the number of peptide groups with the electric dipole $p_0 = 3.5D$, for helix and sheet, respectively.

The stability of the polymer PEDOT-PSS is due to electrostatic interactions between the positively charged thiophene rings of PEDOT units and the negatively charged sulfonate groups of the PSS chain during the polymerization process of PEDOT in PSS solution. The resulting structural organization consists of nearly spherical nanoparticles in solution, in which PEDOT chain segments are bounded to the long of PSS chains. Adding a polar solvent (i.e., ethylene glycol EG, dimethyl sulfoxide DMSO) induces a new organization rich in PEDOT chains as ellipsoidal nanoparticles [29]. In these conditions, the electrical conductivity increases by several orders of magnitude [30, 31]. The two components of the polymer have very different properties. Thus, while PSS is an insulator and has hydrophilic behavior [31], PEDOT is almost conductive and polar, with a resultant electric dipole moment of the repeating unit consisting from 1,4-ethyldioxithiophene and thiophene, oriented perpendicular on PEDOT chain, of 1,87D+0,67D [32]. Also, with the polar solvent addition in initial emulsion the hydrophobic interactions between the PEDOT polar chains and the polar groups of the solvent are enhanced [29]. In this case in PEDOT-PSS polymer's emulsion two phases coexist, one insulating, rich in PSS, and the other conductive with a high concentration of PEDOT-PSS particles. The spin coated film from the PEDOT-PSS emulsion has a granular structure consisting of PEDOT-PSS ellipsoidal nanoparticles with dimensions reported to surface, $d_{parallel}$ ~20-25nm and $d_{vertical}$ ~5-6nm [33], separated lateral and vertical by PSS-water phase sheets. This film surface structure favors a strong anisotropy in terms of conductivity, namely that in surface plane is smaller than that vertical.

The topography images of the BSA/Ag/Si, PEDOT-PSS/Ag/Si, and BSA:PEDOT-PSS[1:1]/Ag/Si films show (Figure 1, right) a granular nanostructured morphology. In order to characterize the geometry of the deposited nanoparticles, we considered the Z parameter value from Table 1 as the vertical diameter $d_{vertical}$, and the surface plane diameter $d_{surface}$, defined as lateral extension of only one maximum from the repetitive maxima group on the corresponding profile curve (Figure 5, middle). The considered intervals for the repetitive maxima group (marked on the profile curves) contain 4 maxima for BSA/Ag/Si, 4 maxima for PEDOT-PSS/Ag/Si and 2 maxima for BSA:PEDOT-PSS[1:1]/Ag/Si films, so that $d_{surface}$ has 55nm, 71nm, 57nm, respectively (Table 1). Axial ratio $d_{vertical}/d_{surface}$ values from Table 1, can be associated to an ellipsoidal nanoparticle, highly elongated in the surface plane for all deposited films. We can assume that the horizontal extension of the molecules in BSA nanoparticles is due to the parallel orientation in surface plane of the helix dipole moments prevalent in elongated BSA molecules, and that the horizontal extension of the PEDOT chains is due to the parallel orientation of the ring dipoles to each other but perpendicular to the film surface. Given the above considerations, both the BSA and PEDOT-PSS nanoparticle films expose polar groups (polar residues of BSA, polar chains of PEDOT-PSS), so that both surfaces are strongly hydrophobic.

To characterize the structural organization of the BSA:PEDOT-PSS[1:1] nanoparticles, we must consider that the BSA molecules and PEDOT-PSS particles may interact both electrostatic between the charged side chain of BSA and sulfonate groups of PSS-water, and also by dipole-dipole interactions between the BSA helices and the PEDOT chains resultant dipole moments. During the spin coating deposition, through partial water elimination, two processes occur: PEDOT-PSS segregation in PEDOT-PSS rich, in PEDOT nanoparticules and PSS-water, and also the elongation of BSA molecule accompanied by the exposure of the hydrophobic groups. Thereby, the dipole-dipole interactions between BSA molecule and PEDOT-PSS rich in PEDOT nanoparticles become prevalent. It is shown [31,33], that the interaction of PEDOT rings dipole with polar groups from solvent, changes the orientation of the PEDOT rings plane, enhancing a strong anisotropy of the film conductivity. Therefore, we can assume that from the BSA:PEDOT-PSS[1:1] emulsion are deposited nanoparticles consisting from the BSA molecules functionalized with a layer of PEDOT chains through dipole-dipole interactions between the BSA (helix) and the PEDOT (rings) dipoles leading to the orientation of the PEDOT rings parallel with the BSA molecule surface, so that the mixture film surface has pronounced hydrophobic properties.

An analysis of the properties and size of the BSA:PEDOT-PSS[1:1] film nanoparticles can be achieved by examining the nature of the tip/surface interaction that leads to the detection of the attractive forces in the snap-off region. If we assume that the tip/surface interaction obeys the Lennard-Jones potential law [34], then the distance d_0 for the maximum value of the detected force in contact/snap-off situation is defined as $d_0 = \sigma_{eff}/2=(\sigma_{tip} + \sigma_{nanoparticle})/2$, while the equilibrium is reached at $d_{ech} = (2)^{1/6}\sigma_{eff}$. The estimated values of the nanoparticule diameters as $\sigma_{nanoparticle} =2d_0-\sigma_{tip}$ for all prepared films are represented in Table 2. These values show that BSA:PEDOT-PSS[1:1] nanoparticles have an average diameter slightly larger than that of the BSA nanoparticles, but much lower than that of PEDOT-PSS rich in PEDOT nanoparticles. On the other hand, the snap-off force of the BSA:PEDOT-PSS[1:1] film is slightly lower than for BSA, but significantly higher than for PEDOT-PSS films. Thus, the tip/BSA:PEDOT-PSS[1:1] film surface interaction is slightly attenuated compared to that with BSA film, more probable due to the interposed PEDOT-PSS film.

Raman spectroscopy is a very precise tool for the biological investigations because it provides accurate data about the biomolecule structures. The protein Raman spectra show specific vibration modes of a particular secondary structure into a tertiary structure organization. Thus, the protein Raman spectrum contains peaks corresponding to the nine vibration modes associated to the peptide unit of the secondary structures α-helix, β-sheet, turn or unordered, structured in Amide I energy band (80% C = O stretch, at ~ 1650 cm^{-1}), Amide II band (60% N - H bend and 40% C - N stretch at ~ 1550 cm^{-1}) and Amide III (40% C-N stretch and 30% N-H bend at ~1300 cm^{-1}), specific peaks attributed to aromatic amino acids (Trp, Tyr, Phe, Hys) vibration modes and peaks attributed to specific vibration modes of S-S bonds which stabilizes the protein tertiary structure [35].

A comparative analysis of the RR spectra shown in Figure 3a reveals that the BSA:PEDOT-PSS[1:1] film RR spectrum cumulates peaks from both BSA and PEDOT-PSS RR spectra. Thus, in the Amide I energy band 1200 – 1800 cm^{-1} region, the BSA:PEDOT-PSS[1:1] film RR spectrum has a single broadband structure, while both BSA and PEDOT-PSS RR spectra have narrow peaks, suggesting a new molecular structure organization of BSA:PEDOT-PSS[1:1]. In Figure 3b the peaks obtained by the broadband band deconvolution are shown. First, in the BSA:PEDOT-PSS[1:1] film RR spectrum, the PSS modes at 701 cm^{-1} is missing, and the PSS modes at 1564 cm^{-1}, 1100 cm^{-1} and 1000 cm^{-1} have much smaller amplitude, suggesting that the new molecule has very low PSS component content [24,25]. In the high energy range, the BSA:PEDOT-PSS[1:1] film RR spectrum contains both α-helix and β-sheet secondary structures peaks, but lacking the short-connecting α-helix chain vibration modes [21-23]. This fact proofs that in the new molecular organization the tertiary structure of the BSA molecule is modified, which is possible by S-S bonds cleavage.

The 1656 cm^{-1} peak associated to α-helix structure mode of BSA, is found as 1656 cm^{-1} peak in the BSA:PEDOT-PSS[1:1] film RR deconvoluted spectrum, so that the new structure inherits α-helix BSA secondary structure content. The 1606 cm^{-1} peak found in BSA:PEDOT-PSS[1:1] film RR spectrum, can be attributed to 1610 cm^{-1} Phe mode from BSA film RR

spectrum, shifted with 4 cm^{-1} due to a new Phe neighborhood [21-23]. The most intense 1508 cm^{-1} deconvoluted peak found in BSA:PEDOT-PSS[1:1] film RR spectrum is found also in as recorded PEDOT-PSS film RR spectrum, where was assigned to symmetric intra-ring mode of PEDOT chains [28,29]. This fact suggests that the PEDOT component is predominant in new molecular structure. The 1432 cm^{-1} deconvoluted peak found in BSA:PEDOT-PSS[1:1] film RR spectrum can be considered coming from the interaction between higher (1449 cm^{-1}) side-chain CH – deformational mode of BSA and lower (1438 cm^{-1}) intra-chain stretching mode of PEDOT chains from PEDOT-PSS, suggesting the association between BSA α-helix structures and PEDOT chains. The 1368 cm^{-1} deconvoluted peak found in BSA:PEDOT-PSS[1:1] film RR spectrum is the same with the 1367 cm^{-1} C_{β}- $C_{\beta'}$ inter-chain rings peak from PEDDOT-PSS film RR spectrum, while the 1320 cm^{-1} deconvoluted peak from BSA:PEDOT-PSS[1:1] film RR spectrum is the lower shift of 1340 cm^{-1} mode assigned to Trp and side-chain CH – deformational mode of BSA film RR spectrum. For protein Raman spectrum, the peaks at 1368 cm^{-1} and 1320 cm^{-1} are related to the Fermi doublet of Trp, and the I_{1368}/I_{1320} intensities ratio is a marker of the Trp neighborhood hydrophobicity [35]. Figure 3b shows that $I_{1368}/I_{1320}>1.1$, and we can conclude that the surface sites occupied by Trp has a predominant hydrophobic neighborhood. This Trp behavior is favorized by PEDOT rings adhesion on BSA chains. The 1266 cm^{-1} deconvoluted peak found in BSA:PEDOT-PSS[1:1] film RR spectrum was not found in BSA film RR spectrum, but can be assigned to shifted 1256 cm^{-1} C_{α} - $C_{\alpha'}$ inter-chain mode found in PEDOT-PSS film RR spectrum. This fact proofs that PEDOT-PSS adheres to BSA molecule by PEDOT chains.

The 1205 cm^{-1} peak found in BSA:PEDOT-PSS[1:1] film as recorded RR spectrum is the lower shift of 1240 cm^{-1} peak found for BSA film RR spectrum, as lower limit of Amide III energy band, assigned to β-sheet vibration modes. The 1125 cm^{-1} and 1031 cm^{-1} peaks found in BSA:PEDOT-PSS[1:1] film as recorded RR spectrum are the same values of Trp modes found in BSA film RR spectrum, proofing that these aromatic amino acids bands are nearly independent of the PEDOT chains (1132 cm^{-1}) and of the PSS (1100 cm^{-1}) neighborhood. We have the same comments for the 1001 cm^{-1} Phe, 850, 827 cm^{-1} Tyr, 620,640 cm^{-1} Phe and 510 cm^{-1} Cys found in BSA:PEDOT-PSS[1:1] film RR spectrum [21-23]. The last three lower energy peaks found in BSA:PEDOT-PSS[1:1] film RR spectrum can be attributed to new S-S bond vibration modes. Thus, the 576 cm^{-1} is a C-S-C deformed PEDOT ring mode, 510 cm^{-1} is the S-S (Cys-Cys) bond mode found in BSA film RR spectrum, and 438 cm^{-1} peak is the S-S bond PEDOT inter-rings mode. The above Raman measurements are in good agreement with the AFM – EFM concluded results and support the development of a new model for the molecular organization of the BSA:PEDOT-PSS[1:1], obtained mainly through the adhesion of the PEDOT chains to the BSA molecule via dipole – dipole interaction between PEDOT rings and BSA peptide chains.

5. Conclusions

Comparative analysis of the AFM measurement results, consisting of simultaneously recorded topography and electrostatic images, profile curves and F(z) curves, for the BSA, PEDOT-PSS and BSA:PEDOT-PSS[1:1] films deposited by spin coating technique on Ag/Si support show that the BSA:PEDOT-PSS[1:1] mixture film exposes a compact surface with a higher roughness than of BSA film, but lower than of PEDOT-PSS film, with amphiphilic properties and more pronounced hydrophobic properties than of both BSA and PEDOT-PSS film surfaces.

Raman spectroscopy results show that the BSA:PEDOT-PSS[1:1] molecule inherits parts from the structure of BSA (α-helix) and PEDOT-PSS (PEDOT chains), assembled into new molecular structure. The structure of the BSA:PEDOT-PSS[1:1] molecule is stabilized by overlapping the main vibrational modes from Amide I energy band of BSA with the intra-ring and/or intra-chains of PEDOT-PSS. The recorded specific modes show that Trp, Tyr, Phe occupy active positions as well as in the BSA molecule. The recorded S – S bonds vibrational modes sum both the S – S bond in BSA and the S – S bond obtained by the interaction between BSA (Cys) and PEDOT rings (C – S – C) vibration modes.

Taking into account the above remarks, we can conclude that the obtained BSA:PEDOT-PSS[1:1] mixture has some properties that respond to bioactive layer requests: a) increased surface polarity by the dipole (protein) – dipole (polymer) interactions and predominant hydrophobic properties, ensuring greater stability in the fluid sample; b) higher conductivity due to great PEDOT chains content; c) surface active sites occupied by aromatic amino acids, which allows the analysis of a fluorescent response; d) surface sites activated by S-S bonds. The BSA:PEDOT-PSS[1:1] film, exposed to biological fluid sample, living or cells culture, can assure an efficiently adhesion for small biomolecules, polar or charged groups. While the BSA component ensures the improvement of composite biocompatibility, PEDOT-PSS component provide the stability and flexibility of the BSA:PEDOT-PSS[1:1] bioactive layer.

Acknowledgement

The work has been funded by the Sectoral Operational Program Human Resources Development 2007-2013 of the Ministry of European Funds through the Financial Agreement POSDRU/159/1.5/S/137750

References

[1] N. Jalili, K. Laxaminarayana, Mechatronics **14**, 907 (2004)
[2] N.A. Peppas, R. Langer, Science **263**, 1715(1994)
[3] R.A. Lewis, A.R. Leach, J. Computer Aided Mol. Des. **8**, 467 (1994)
[4] A. Antognozzi, et al., Nanotech., **17**, 3897 (2006)
[5] P. Pingue, et al., Appl. Phys. Lett., **88**, 043510 (2006)
[6] R.E. Olson, D.D. Christ, Ann. Rep. Med. Chem. **31**, 327 (1996)
[7] M. Dieaconu, A. Ioanid, S. Iftimie, S. Antohe, Dig. J. Nanomater. Bios., **7**, 1125 (2012)
[8] J. Valanciunaite, S. Bagdonas, G. Streckyte, R. Rotomskis, Photochem. Photobiol. Sci. **5,** 381 (2006)
[9] M. Dieaconu, A. Ioanid, S. Antohe, Dig. J. Nanomater. Bios., **8**, 89 (2013)
[10] A. Ioanid, S. Antohe, Digest J. Nanomat. Biostruct., **8**, 1633 (2013)
[11] A.G. MacDiarmid, Angew. Chem. Int. Ed., **40**, 2581(2001)
[12] E. Mikamo-Satoh, F. Yamada, A. Takagi, T. Matsumoto, T. Kawai, Nanotech. **20**, 145102 (2009)
[13] H.P. Erickson, Biol. Proced. Online, **11**, 32 (2009)
[14] A. Ioanid, M. Dieaconu, S. Antohe, J. Optoelectron. Adv. Mater., **13**, 1470 (2011)
[15] M. Venkataramanan, G. Skanth, K. Bandyopadhyay, K. Vijayamohanan, T. Pradeep, J. Colloid Interface Sci., **212**, 553 (1999)
[16] A.M. Nardes, et al, Adv. Mater., **19**, 1196 (2007)
[17] H.J. Butt, B. Cappella, M. Kappl, Surf. Sci. Rep. **59**, 1 (2005)
[18] C.C. Lai, N. Motta J.M. Bell, Int. J. Nanosci. **7**, 299 (2008)
[19] A. Ioanid, M. Dieaconu, S. Antohe, Dig. J. Nanomater. Bios., **5**, 947, (2010)
[20] D. Khatiwada, S.K. Lamichhane, Himalayan Phy., **2**, 80 (2011)
[21] G. Navarra, A. Tinti, M. Leone, V. Militello, J. Inorg. Biochem., **103**, 1729 (2009)
[22] H.D. Bing, X.L. Peng, F.P. Huang, D. Yao, Q. Yi, H. Liang, Evid. Based Complement. Alternat. Med. **2014**, 1 (2014)
[23] S.U. Sane, S.M. Cramer, T.M. Przybycien, Anal. Biochem. **269**, 255 (1999)
[24] J. Weszka, M.M. Szindler, P. Jarka, J. Achiev. Mater. Manuf. Eng. **59**, 59 (2013)
[25] A.A. Farah, S.A. Rutledge, A. Schaarschmidt, R. Lai, J.P. Freedman, A.S. Helmy, J. Applied Phys. **112**, 113709 (2012)
[26] N.C. Matiti, M.M. Apetri, M.G. Zagorski, P.R. Carey, V.E. Anderson, J. Am. Chem. Soc., **126**, 2399 (2004)
[27] C. Giancola, C.D. Sena, D. Fessas, G. Garoziano, G. Barone, Int. J. Biol. Macromol. **20**, 193 (1997)

[28] A. Gebregeorgis, C. Bhan, O. Wilson, D. Raghavan, J. Colloid Interface Sci. **389**, 31 (2013)
[29] J. Gasiorowski, R. Menon, K. Hingerl, M. Dachev, N.S. Sariciftci, Thin Solid Films **536**, 211 (2013).
[30] Kim, Yong Hyun, et al, Adv. Funct. Mater., **21**, 1076 (2011)
[31] X. Crispin, F.L.E. Jakobsson, A. Crispin, P.C.M. Grim, P. Andersson, A. Volodin, C. van Haesendonck, M. Van der Auweraer, W.R. Salaneck, M. Berggren, Chem. Mater **18**, 4354 (2006)
[32] J. Ouyang, Q. Xu, C.W. Chu, Y. Yang, G. Li, J. Shinar, Polymer **45**, 8443 (2004)
[33] Nardes, Alexandre Mantovani, et al, Adv. Mater **19**, 1196, (2007)
[34] A. Ioanid, S. Antohe, Dig. J. Nanomater. Bios., **9**, 1223 (2014)
[35] Chen Zhou, Wei Qi, E. Neil Lewis, John F. Carpenter, Anal. Biochem. **472**, 7 (2015)